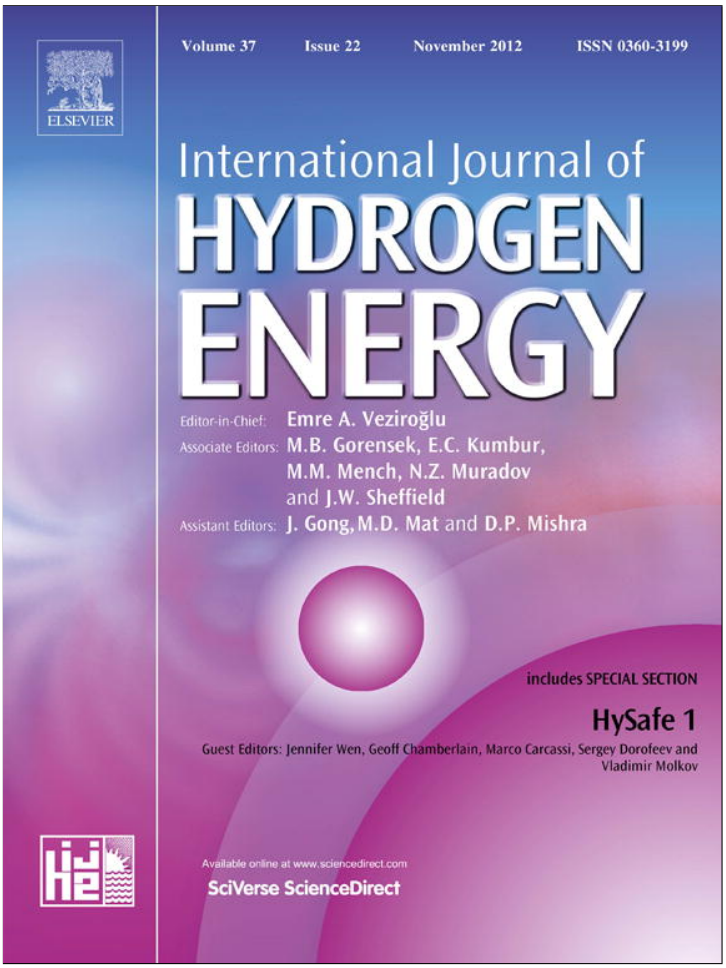

INTERNATIONAL JOURNAL OF HYDROGEN ENERGY 37 (2012) 16844–16851

Available online at www.sciencedirect.com

SciVerse ScienceDirect

journal homepage: www.elsevier.com/locate/he

MgH_2 synthesis during reactive mechanical alloying studied by *in-situ* pressure monitoring

*Facundo J. Castro**, *Valeria Fuster* [1], *Guillermina Urretavizcaya*

Centro Atómico Bariloche (CNEA, CONICET), Instituto Balseiro (UNCuyo, CNEA), Av. Bustillo 9500, R8402AGP, S. C. de Bariloche, Río Negro, Argentina

ARTICLE INFO

Article history:
Received 17 July 2012
Received in revised form
16 August 2012
Accepted 21 August 2012
Available online 18 September 2012

Keywords:
Hydrogen diffusion
Mechanical milling
Magnesium hydride
Synthesis
In-situ

ABSTRACT

The synthesis of MgH_2 by reactive mechanical milling has been studied by monitoring H_2 pressure changes inside a milling chamber. Mg and a Mg-10 wt.% C mixture were used as starting materials and milled under 0.5 MPa of H_2. The addition of C doubles the MgH_2 synthesis efficiency due to C acting as a process control agent. MgH_2 formation has been observed throughout milling and during the rest periods between milling stages. Mg hydriding during the rest periods has been found to be controlled by hydrogen diffusion through MgH_2. High-diffusivity paths along grain boundaries seem to be operative during the process. A lower bound for the diffusion coefficient of H in MgH_2 at room temperature of 10^{-25} m^2 s^{-1} has been estimated from the data.

1. Introduction

In the last years Mg and its hydride have been extensively studied due to their potential application to store hydrogen [1–7]. MgH_2 main advantages are its low cost and high hydrogen content per mass (7.6 wt.%); its principal drawbacks are its high stability and the extremely slow hydrogen absorption and desorption rates near room temperature. To overcome these disadvantages mechanochemical methods have been successfully employed to obtain Mg-based materials with better hydrogen sorption properties [5,8–10].

Reactive mechanical alloying (RMA) is a mechanochemical technique that allows hydride synthesis by processing the materials under a reactive H_2 atmosphere [11]. Interesting results have been observed when following the RMA process by pressure measurements. Chen et al. were the first to show that MgH_2 formation can be analyzed by monitoring the H_2 pressure decrease inside a milling vial [12]. More recently, Doppiu *et al.* have used the same technique to determine the effect of different H_2 pressures on Mg hydriding by RMA [13]. The synthesis of other hydrides has also been followed by pressure measurements: Chen *et al.* and Dunlap *et al.* have studied the hydriding behavior of Ti [12,14], Friedrichs *et al.* have analyzed the reaction of Mn_3Ti_2V and Ca with H_2 during RMA [15], and likewise Zhang and coworkers have determined the reaction path leading to the formation of Mg_2TM (TM = Fe, Co, Ni) complex hydrides [16]. Interestingly, in a few cases it has been mentioned that the hydriding process not only occurs during milling, but also happens throughout the rest periods between milling stages [12,14]. However, these

* *Corresponding author.*
E-mail addresses: fcastro@cab.cnea.gov.ar (F.J. Castro), vfuster@conicet.gov.ar (V. Fuster), urreta@cab.cnea.gov.ar (G. Urretavizcaya).
[1] Present address: INFIQC-CONICET, Dpto. de Fisicoquímica, Fac. de Ciencias Químicas, Universidad Nacional de Córdoba, X5000HUA, Córdoba, Argentina.

0360-3199/$ – see front matter
http://dx.doi.org/10.1016/j.ijhydene.2012.08.089

processes were not further studied, and their main characteristics remain unknown.

Mg can be hydrided by RMA at room temperature as a result of the generation of free-from-oxide fresh surface and the removal of surface hydride layers that impair further hydriding due to the sluggish H diffusion through MgH_2. Hydrogen diffusion in MgH_2 has been moderately studied up to now [17–23], and the reported results have always been obtained above room temperature. Additionally, it is not yet clear if H diffusion through MgH_2 occurs via a high-diffusivity path along grain boundaries or not.

In this work, we present an analysis of MgH_2 synthesis by RMA from Mg and a mixture of Mg and C. The study is based on hydriding data inferred from *in-situ* pressure measurements. Our results allow us to establish a connection between hydrogen diffusion in MgH_2 and the RMA process.

2. Experimental

Mg (Riedel de Häen, 99%, average size 100 μm) denoted as (Mg) and a mixture of Mg-10 wt.% C (Sigma–Aldrich, 99.9%, platelets, average diameter 200 μm, average thickness 50 μm) designated as (Mg + C) were ball-milled in a Uni-Ball-Mill II apparatus under 0.5 MPa of high-purity H_2. The ball-to-powder mass ratio was 44:1, and the rotational speed was 195 rpm. Constant pressure inside the milling vial was ensured by regularly refilling the chamber. The milling program consisted of milling stages of up to 10 h followed by rest periods of variable duration. *In-situ* pressure measurements were done via an Omega PX-181 pressure transducer. Data were stored in a HOBO H8 data logger attached to the milling chamber. A Bacharach Leakator 10 combustible gas detector was used to check for H_2 leaks. SEM images were obtained with a Philips Electronic Instruments SEM 515. All handlings were done within a Glove box with a purified argon atmosphere with O_2 and H_2O levels below 1 ppm.

3. Results and discussion

3.1. Milling

H_2 pressure inside the milling chamber decreased both throughout milling and during the rest periods (Fig. 1). Pressure decrease during milling is the consequence of H_2 consumption to form MgH_2 in the closed milling vessel. The amount of MgH_2 formed can be deduced at the pressures involved here by applying the ideal gas law. Pressure changes during the rest periods, as will be discussed below, are also due to H_2 consumption to form MgH_2. These last processes were observed regularly, with the exception of the initial milling period of (Mg) and the final stages of (Mg) and (Mg + C) (Fig. 2). Similar observations have been reported in Ti [12,14] and Mn_3Ti_2V [15]. In both cases, pressure drops were attributed to hydride formation.

The reduction in H_2 pressure during the rest periods can be a consequence of: a) H_2 leaks, b) gas cooling and c) hydrogen consumption due to hydride formation. Gas leaks were discarded as the system was thoroughly examined with

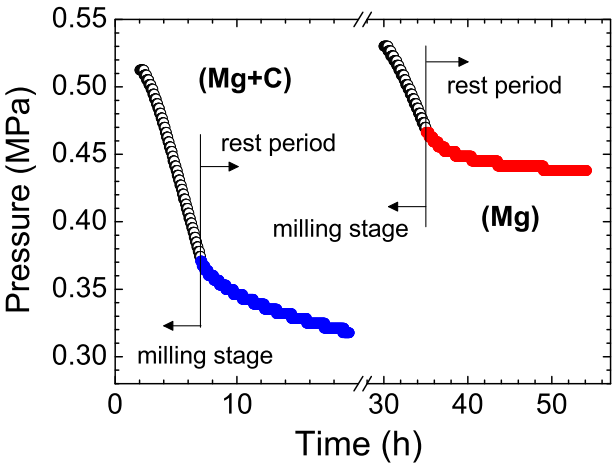

Fig. 1 – Pressure changes inside the milling chamber during milling (open symbols) and resting periods (filled symbols). Error bars are of the order of symbols size.

a combustible gas detector and no leaks were detected. Besides, the observed saturation pressure (the final pressure at the end of the drop during the rest period) is well over ambient pressure (Fig. 1). Gas cooling would be the natural consequence of gas heating during mechanical processing. It has been reported that the temperature of milling chambers and balls can increase noticeably when milling is performed with intermediate or high-energy milling devices [13,16,24]. Several processes contribute to the heating of the milling media: mechanical energy converted into heat, MgH_2 formation reaction, Mg plastic deformation, etc. However, the temperature increase in the case of this low-energy miller is rather small. After a typical milling stage, the temperature of the external part of the chamber did not exceed room temperature by more than 3 °C. Additionally, the pressure drops are less pronounced after the later milling stages and even disappear for the last stages (Fig. 2), contradicting the possibility of the pressure drops being a consequence of gas cooling. The

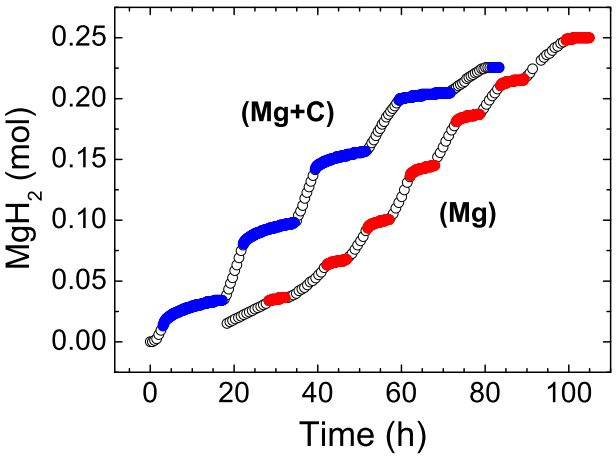

Fig. 2 – Amount of MgH_2 formed during the mechanochemical treatment. The figure includes milling periods (open symbols) and resting intervals (filled symbols). Error bars are of the order of symbols size.

absence of a substantial increase in temperature (and posterior cooling) can be attributed to an efficient heat dissipation process resulting from the combination of a reduced milling energy, the high thermal conductivity of H_2, and the large milling chamber volume (~0.8 l) and mass (~8 kg), the latter compared with the milled powder mass (~7 g). This was quantitatively confirmed by an estimation of the timescale of the heat dissipation process, as we did not have the possibility to measure gas temperature inside the chamber. We have calculated a characteristic time associated with the cooling process of the hydrogen mass contained in the milling chamber of the order of minutes, taking into account the thermal properties of hydrogen at the milling pressure and the chamber dimensions. This value is considerably shorter than the timescale of 10–20 h observed in the pressure drops during the rest periods. The estimated timescale agrees well with the typical times experimentally observed in a different milling device, with a small chamber but a higher milling energy [16]. Therefore, having discarded gas leaks and gas cooling as causes of pressure drops, we attribute pressure changes to H_2 consumption by MgH_2 formation.

3.2. *Hydriding during milling period*

Fig. 3 shows the amount of MgH_2 formed in (Mg) and (Mg + C) without considering the pressure changes registered during the rest periods. Both curves have a sigmoidal shape. Similar shapes have been reported for Mg [12,13,25], Ti [14] and Ca [15]. The induction period is associated with the microstructural refinement necessary for hydriding to begin [13,14]. The final stage is related to magnesium exhaustion. Overall, we observe that (Mg + C) needs almost half the time required for (Mg) to be fully hydrided. To be able to extract more information from the curves, a simple model for the process is developed. The model considers three species: Mg, Mg* ("activated" Mg) and MgH_2. Mg represents the starting material, not yet modified by milling, Mg* describes Mg "activated" by the mechanical process and MgH_2 denotes the hydride formed from the reaction of Mg* with H_2. Mg* has a microstructure modified by the milling process, and more importantly, a fresh surface, free from

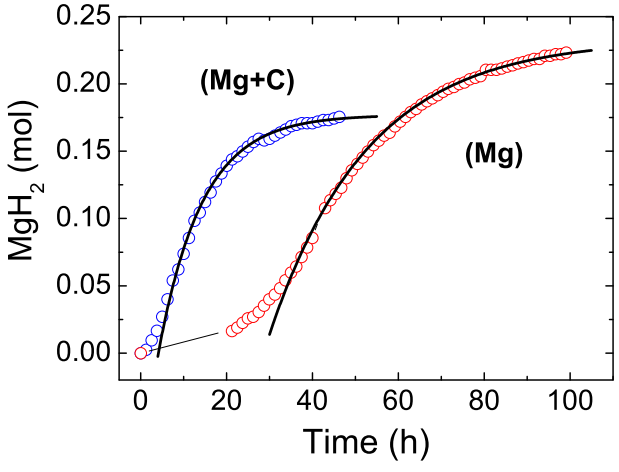

Fig. 3 – MgH_2 amount in (Mg) and (Mg + C) formed during milling. Error bars are of the order of symbols size.

oxides and previously formed MgH_2 layers. The hydriding process is modeled by a series reaction schematized as:

$$Mg \rightarrow Mg^*$$

$$Mg^* + H_2 \rightarrow MgH_2$$

During these reactions, Mg* acts as an intermediate species that is produced in a characteristic time τ_m by mechanically processing Mg, and is consumed by reacting with hydrogen to produce MgH_2 in a characteristic reaction time τ_r. The reaction rates of Mg, Mg* and MgH_2 are given by:

$$\frac{dN_{Mg}}{dt} = -\frac{N_{Mg}}{\tau_m} \quad (1)$$

$$\frac{dN_{Mg^*}}{dt} = \frac{N_{Mg}}{\tau_m} - \frac{N_{Mg^*}}{\tau_r} \quad (2)$$

$$\frac{dN_{MgH_2}}{dt} = \frac{N_{Mg^*}}{\tau_r} \quad (3)$$

where N_{Mg}, N_{Mg^*} and N_{MgH2} represent the number of moles of Mg, Mg* and MgH_2, respectively. The characteristics of the general solution of this model are well-known [26]. In this particular case, the experimental data after the induction period can be very well fitted with the expression:

$$N_{MgH_2}(t) = N_F\left(1 - e^{-t/\tau}\right) \quad (4)$$

that corresponds to the limiting cases of a milling controlled process ($\tau_r << \tau_m$) or a hydriding reaction controlled process ($\tau_m << \tau_r$). In Eq. (4) N_F represents the final amount of MgH_2 and τ is either τ_r or τ_m, depending on the specific rate controlling process. The hydriding rate from Eq (4) is

$$\frac{dN_{MgH_2}}{dt} = \frac{N_F}{\tau} e^{-t/\tau} \quad (5)$$

and in terms of the conversion fraction

$$\alpha = \frac{N_{MgH_2}}{N_F} = 1 - e^{-t/\tau} \quad (6)$$

it is given by

$$\frac{dN_{MgH_2}}{dt} = \frac{N_F}{\tau}(1 - \alpha) \quad (7)$$

Eq. (7) shows that the rate is proportional to the unreacted fraction $(1 - \alpha)$.

The fitted τ values are 23 h for (Mg) and 10 h for (Mg + C). Taking into account that we are using a low-energy milling device and that MgH_2 formation by RMA can be completed in much less than 50 h [12,13,25], it seems that the hydriding process here is controlled by milling. Within this interpretation, τ corresponds to τ_m, and the shorter timescale observed for (Mg + C) can be attributed to C acting as a process control agent. This is achieved by the well-known C lubricating properties that limit cold-welding.

3.3. *Hydriding during the rest periods*

Mg hydriding data during the rest periods present a different time-dependence (Fig. 4). Data was very well fitted with a function of the form

$$N_{H_2} = N_0 + (Bt)^{\frac{1}{2}} \quad (8)$$

where N_{H_2} is the hydrogen content of the material, N_0 is the hydrogen initial amount and B is a coefficient whose physical meaning is discussed below (see Eq. (17)). The parabolic time-dependence suggests a diffusion-limited process. A possible scenario is the following. During milling Mg hydriding is controlled by the milling rate, by means of the fresh surface creation rate. Once milling is stopped, and the rest period begins, the formation of fresh surface ends and only a fraction of Mg exposes a clean surface to H_2. This fraction is the main part of the material that is going to be hydrided during the rest period. Hydriding starts on the surface and advances towards the interior forming a hydride layer that grows in depth. This process assumes that many nuclei are formed on the surface to ensure the establishment of a hydride layer. Within this picture, further hydriding can only occur by hydrogen diffusion through the hydride layer, which due to the well-known slowness of the process [17–23] will naturally control the whole hydriding process. An idealized diagram of the model is schematized in Fig. 5. A spherical particle of radius R_0 is hydrided by being exposed to an external hydrogen pressure p_{H2}. The particle has an external MgH_2 shell that extends from the surface down to r_i, where the interface between MgH_2 and Mg is located. The internal region of the particle is composed of unhydrided Mg. As hydrogen diffuses through the hydride, the interface moves towards the interior of the particle and the surrounding hydride layer grows. Recalling that the amount of hydride that forms during the rest periods is a small fraction of the total amount of MgH_2 (Fig. 2), the depth of the hydride layer grown during the rest periods can be considered much smaller than the radius of the particle. This assumption allows us to model hydriding as a one-dimensional process. By additionally assuming a steady state solution, the hydrogen diffusive flow through the hydride layer is given by:

$$J = Mc\frac{d\mu}{dx} \approx Mc_{MgH_2}\frac{\mu(R_0) - \mu(r_i)}{R_0 - r_i} \quad (9)$$

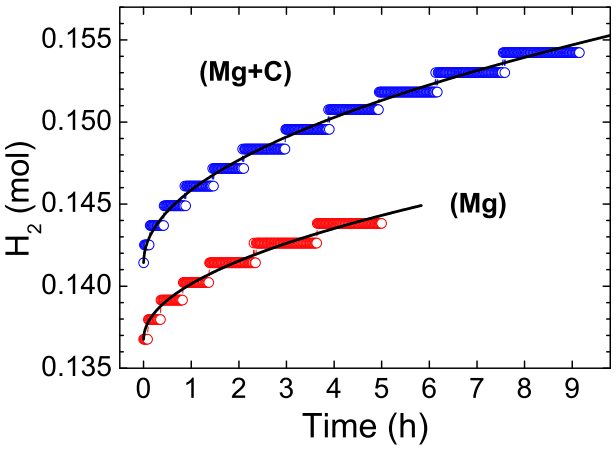

Fig. 4 – Hydrogen content in (Mg) and (Mg + C) during typical rest periods. The fits follow Eq. (8). The jumps in the experimental values are due to the data acquisition system discretization.

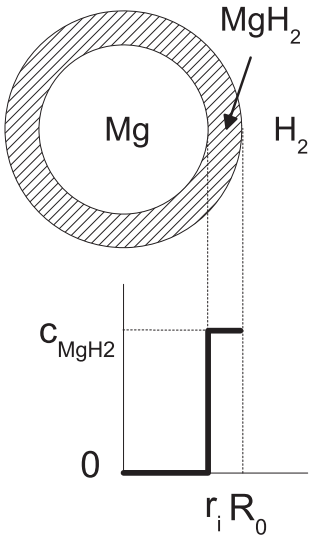

Fig. 5 – Scheme of the hydriding process model.

where μ is the hydrogen chemical potential, M the hydrogen mobility and c_{MgH2} the hydrogen concentration in MgH_2, assumed to be approximately the same in R_0 or in r_i (there is no appreciable H_2 solubility in MgH_2 [27,28]). The amount of hydrogen in the particle, neglecting H solubility in Mg [27,28], can be given by

$$N_{H_2} = Ac_{MgH_2}(R_0 - r_i), \quad (10)$$

where A is the area of the particle of radius R_0 (hydride layer thickness much smaller than the particle radius). The time derivative of Eq. (10) connects the hydriding rate with the interface velocity.

$$\frac{dN_{H_2}}{dt} = -Ac_{MgH_2}\frac{dr_i}{dt}. \quad (11)$$

On the other hand, the hydriding rate is proportional to the hydrogen flow through the hydride layer.

$$\frac{dN_{H_2}}{dt} = AJ. \quad (12)$$

using the following expression for the chemical potential.

$$\mu(R_0) - \mu(r_i) = \frac{RT}{2}\ln\left(\frac{p_{H_2}}{Peq}\right), \quad (13)$$

and combining Eqs. (9) and (11)–(13), the temporal evolution of r_i can be obtained as

$$r_i(t) = R_0 - \left[D\ln\left(\frac{p_{H_2}}{peq}\right)t\right]^{\frac{1}{2}}, \quad (14)$$

where D denotes the tracer diffusion coefficient, equal to the product MRT. Replacing Eq. (14) in Eq. (10), the amount of hydrogen in the hydride is obtained as

$$N_{H_2}(t) = Ac_{MgH_2}\left[D\ln\left(\frac{p_{H_2}}{peq}\right)t\right]^{\frac{1}{2}}. \quad (15)$$

This expression has been derived for one particle. Its generalization to the whole sample can be made by replacing

A by A_{eff}, the area of Mg "activated" by milling corresponding to the whole sample. The "activated" fraction is taken into account by the factor γ, and the fraction of the total surface that corresponds to Mg by the hydriding degree α. The effective total area is then given by:

$$A_{eff} = \gamma A_0(1-\alpha), \tag{16}$$

where A_0 is the total area of the sample. Replacing A by A_{eff} in Eq. (15), the expression for the amount of hydrogen in the material takes the form:

$$N_{H_2}(t) = \left[D\gamma^2 A_0^2 (1-\alpha)^2 c_{MgH_2}^2 \ln\left(\frac{p_{H_2}}{p_{eq}}\right) t\right]^{\frac{1}{2}}. \tag{17}$$

By fitting our data with Eq. (17) we have calculated $D\gamma^2A_0^2$ (Fig. 6). We observe a good agreement between the values corresponding to different (Mg) samples, showing a very good repeatability. We also note that the (Mg + C) values are slightly higher than those of (Mg). Additionally, we see an increase in $D\gamma^2A_0^2$ as the conversion fraction approaches unity, more pronounced for (Mg) than for (Mg + C). The increase in $D\gamma^2A_0^2$ can be attributed to the increase in A_0, due to the size reduction consequence of milling.

To estimate the value of A_0 we have considered two possible scenarios: a first one in which diffusion takes place in the Mg particles that compose the sample, and a second one in which hydrogen diffusion through grain boundaries is much faster than bulk diffusion, and the effective particles into which hydrogen is diffusing are the crystallites. Particle area for the first situation has been estimated from SEM images (Fig. 7), while grain boundary area for the second option has been calculated from grain size data estimated from XRD results [29]. In both cases, the following expression for the total surface of a sample of mass m and density ρ, composed of a great number of spherical particles of radius R_0 has been used.

$$A_0 = \frac{3m}{\rho R_0} \tag{18}$$

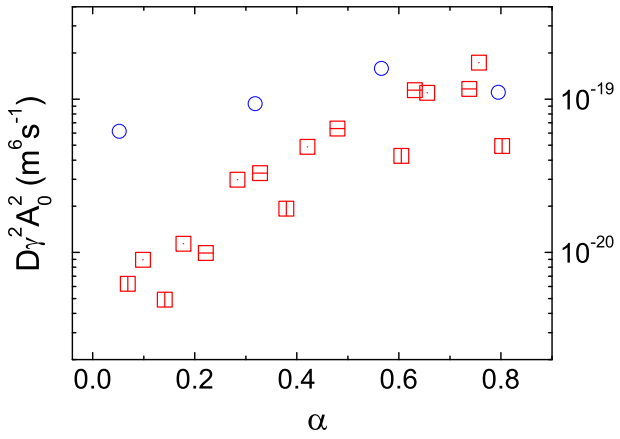

Fig. 6 – Values of $D\gamma^2A_0^2$ obtained by fitting the hydriding data during rest periods. Circles correspond to (Mg + C) and squares to (Mg). Three different (Mg) samples have been measured; each sample is identified by distinct square symbols.

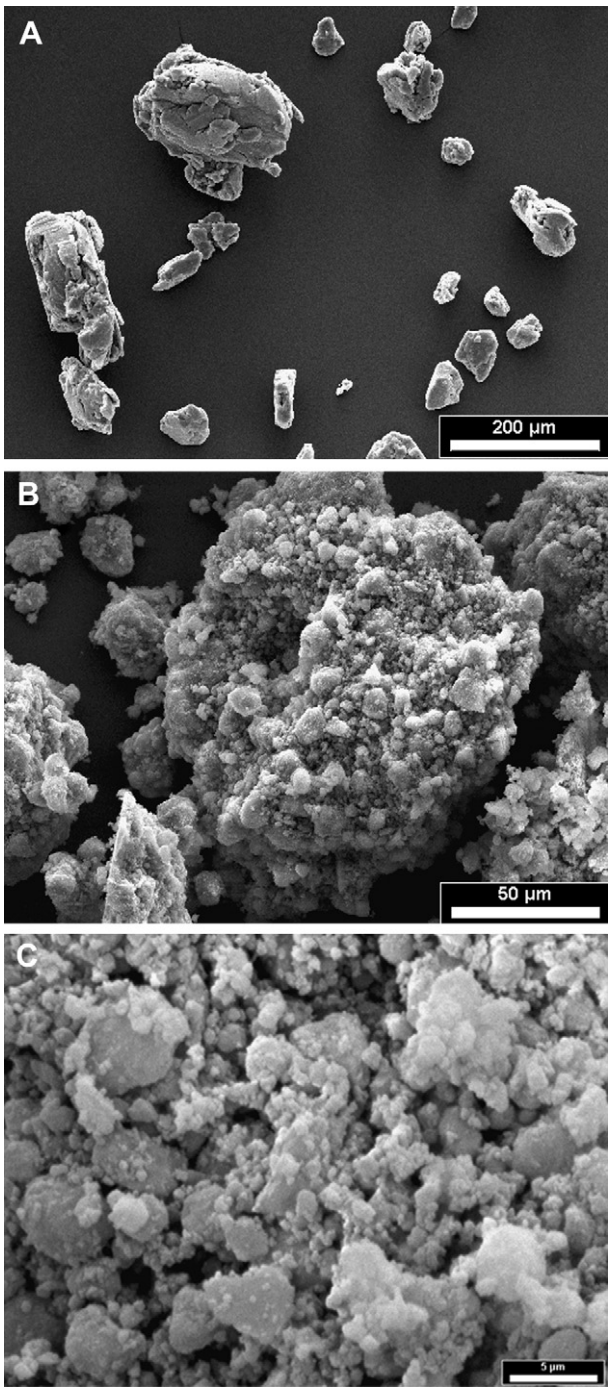

Fig. 7 – SEM images exemplifying particle-size changes with milling in (Mg). A: 12 h (α = 0.07), B: 50 h (α = 0.6) and C: 100 h (α = 1).

The A_0 values associated with each scenario are presented in Fig. 8. It can be seen that the square of crystallite area spans a range of almost one order of magnitude, whereas particle area extends over nearly four orders of magnitude. As the $D\gamma^2A_0^2$ values range over one order of magnitude, and there are no reasons to expect a decrease in D or a change in γ as the conversion fraction grows, a diffusion process in which the effective particles are the crystallites is assumed. Therefore,

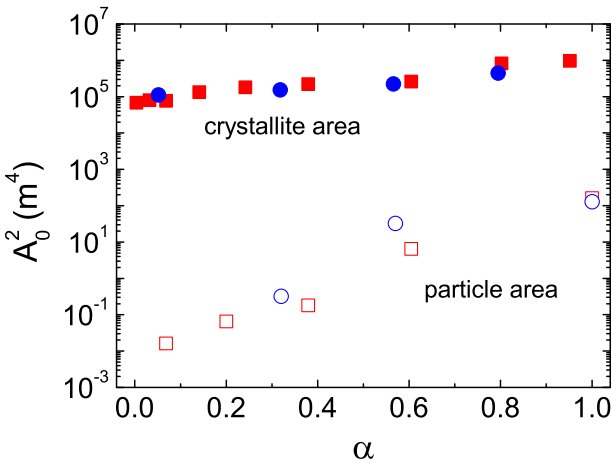

Fig. 8 – A_0 values corresponding to particle area (open symbols) and crystallite area (filled symbols) as a function of the conversion fraction. Square symbols correspond to (Mg) and circles to (Mg + C).

a lower bound for D, denoted as D_{LB}, can be estimated by setting γ equal to 1 (Fig. 9). The observed data dispersion is narrower than that of Fig. 6, suggesting that a rapid mobility along grain boundaries, together with the crystallites being the effective particles for diffusion could be the correct explanation. A similar idea has been proposed by [16,20–22,30,31]. A slight increasing trend in D_{LB} values is observed for (Mg) as α goes up to 0.6. At this value, (Mg) and (Mg + C) data roughly coincide. The increasing D_{LB} values for (Mg) can be linked with the microstructural evolution of the sample during milling. This trend is less evident for (Mg + C) as a consequence of the more efficient milling process. The relationship between microstructural refinement and diffusion is the defect mediated H diffusion process that takes place in MgH_2 [32]. For α beyond 0.6, D_{LB} values for both materials slightly decrease. We interpret this as our simplified

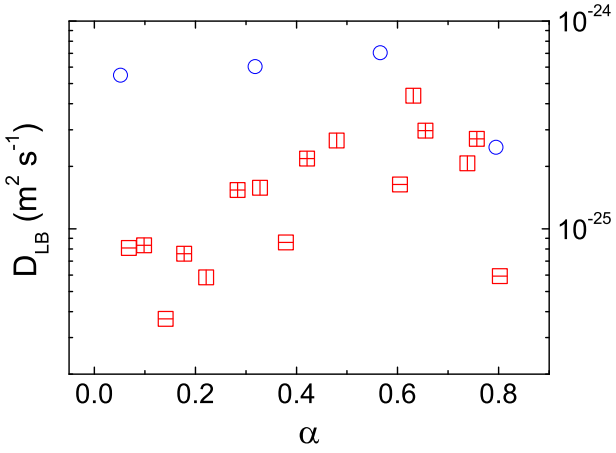

Fig. 9 – Lower bound value for the diffusion coefficient of H in MgH_2. Circles correspond to (Mg + C) and squares to (Mg). Different (Mg) samples are identified by distinct square symbols.

model failing to represent the process when the material is almost fully hydrided. Taking all this into account, a value of 10^{-25} m^2 s^{-1} can be taken as a rough estimation of D_{LB}. To the best of our knowledge, there are no reports of D values measured at room temperature, but this lower bound for H diffusion in MgH_2 at room temperature can be compared with D values extrapolated from data measured at higher temperatures. We have found three different D data sources: 1) D values deduced from fitting macroscopic hydrogen absorption and desorption curves with kinetic models that consider diffusion as a rate controlling step [21–23], 2) D values obtained from nuclear magnetic resonance measurements of H hoping rate in MgH_2 [19,20] and 3) D values determined from first principles calculations [32]. With the exception of the calculated data, that cover a temperature range that includes room temperature, the extrapolated D values have been obtained by using an Arrhenius dependence with the corresponding parameters reported in each reference. In the case of the D values estimated from the H hoping rate, the diffusion coefficient has been calculated by us assuming the H diffusion pathway reported in [32].

As can be seen in Table 1, literature data span a range from 10^{-35} to 10^{-21} m^2 s^{-1}. Our determination is well within the range of group 1) values, obtained from hydrogen absorption and desorption measurements. Moreover, the value from [21], the only one that corresponds to MgH_2 without additives, can be matched by setting γ equal to 0.01. This γ value implies that 1% of the surface is "activated" by milling in each milling event, a more realistic assumption than setting γ equal to 1. The NMR values corresponding to coarse grained MgH_2 are consistently below our lower bound for D, which is reasonable considering the microstructural differences between that material and our ball-milled powders. Additionally, our value could also be incremented by extrinsic defects due to impurities potentially present in the starting Mg [20]. For the same reasons mentioned above, D values obtained from first principles calculations performed on bulk MgH_2, are also below our lower bound. Interestingly however, first principles calculations predict the coincidence of the D values obtained for (Mg) and (Mg + C). In [33] it is reported that graphite is incorporated as a neutral dopant in MgH_2, and as such, it does not change the concentration of defects because it does not alter the charge neutrality in the material. Therefore, H diffusion should not change by the addition of C to MgH_2, as is found here.

3.4. *Hydriding process, general description*

We can now try to connect the diffusion-limited hydriding process taking place throughout the rest periods with the MgH_2 synthesis that occurs during milling. An extremely simplified model is considered. When the material is milled, several milling events such as ball-to-ball collisions and ball-to-chamber impacts modify the material so as to create fresh surface, by separating the previously formed hydride layers from the external parts of the material. Between two milling events, it can be assumed that hydriding proceeds through a diffusion-limited process similar to the one observed during the rest periods. Each time a milling event occurs, a new diffusion process starts. This process continues

Table 1 – Values of the hydrogen diffusion coefficient in MgH_2 estimated from literature data.

D @ 294 K ($m^2\ s^{-1}$)	System	Method	Temperature range (K)	Ref
1.4×10^{-25}	Mg–V nanoblades	Absorption curves fitting	500–570	[23]
1.0×10^{-28}	Mg–FeTi–CNT's	Absorption curves fitting	373–573	[22]
1.3×10^{-21}	MgH_2 powder and foil	Desorption curves fitting	580–700	[21]
3×10^{-35}	coarse grained MgH_2	NMR	533–673	[20]
6×10^{-33}	coarse grained MgH_2	NMR	500–750	[19]
1×10^{-29}	MgH_2	First principles calculation	300–700	[32]

until the next milling event happens. Within this picture, hydriding during milling can be thought as the succession of many short-lived diffusion curves separated in time by τ_{mill}, the characteristic time between two effective milling events (Fig. 10). In a τ_{mill} time the amount of hydrogen incorporated by the sample is given by N_{H2} (τ_{mill}) (Eq. (17)). If τ_{mill} is short enough, the hydriding rate during milling can be estimated as (Fig. 10):

$$\frac{dN_{H_2}}{dt} \approx \frac{N_{H_2}(\tau_{mill})}{\tau_{mill}} \tag{19}$$

in terms of the parameter λ defined as

$$\lambda = \left[D\gamma^2 A_0^2 c_{MgH2}^2 \ln\left(\frac{p_{H2}}{peq}\right)\right]^{\frac{1}{2}} \tag{20}$$

N_{H2} (τ_{mill}) can be written as

$$N_{H_2}(\tau_{mill}) = \lambda(1-\alpha)\tau_{mill}^{1/2} \tag{21}$$

and the hydriding rate during milling is

$$\frac{dN_{H2}}{dt} \approx \frac{\lambda}{\tau_{mill}^{1/2}}(1-\alpha) \tag{22}$$

Considering the stoichiometric molar ratio between H_2 and MgH_2, Eq. (22) can be compared with the macroscopic rate previously derived [Eq. (7)]. Both expressions present the same α dependence, and the link between the phenomenological treatment of Eqs (1)–(3) and the diffusional approach can be made by equating the corresponding coefficients.

$$\frac{N_F}{\tau_m} = \frac{\lambda}{\tau_{mill}^{1/2}} \tag{23}$$

By expressing N_F in terms of c_{MgH2}, A_0 and R_0, and recalling Eq. (18), the following relationship is obtained from Eq. (23):

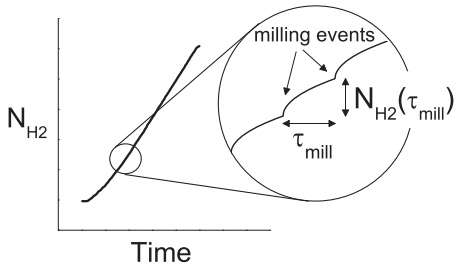

Fig. 10 – Representation of the hydriding process during milling as a sequence of short diffusion-controlled hydriding processes separated by milling events.

$$\tau_m^2 = \frac{\tau_{mill}}{D\gamma^2 A_0^2 \left(\frac{\rho}{m}\right)^2 \ln\left(\frac{p_{H_2}}{p_{eq}}\right)} \tag{24}$$

therefore, the macroscopic timescale τ_m is connected to material properties through D, p_{eq} ρ and A_0, to experimental properties through p_{H_2} and m, and to milling parameters through τ_{mill}. Unfortunately, the characteristics of the milling apparatus employed in this study do not allow us to change the milling rate in order to check experimentally the relationship predicted by Eq. (24). The milling rate and the milling mode are strongly correlated in our device, and it is not possible to change τ_{mill} without affecting the milling mode, and hence altering the whole process. However, Eq. (24) allows us to estimate values of τ_{mill} using the $D\gamma^2A_0^2$ values depicted in Fig. 6 and the τ_m values previously determined. The calculated τ_{mill} values are in the range of 0.5–1 min during the first milling stages and increase up to 4–6 min when α is around 0.6.

As a final remark, we want to mention that we have tried to register hydrogen absorption in (Mg) and (Mg + C) at room temperature using a volumetric device, but no hydriding was observed. The experiments were conducted as follows. The samples were dehydrided in the volumetric apparatus under mechanical vacuum during heating to 325 °C at 5 °C/min, then they were cooled under dynamic vacuum down to 25 °C and finally exposed to 0.5 MPa H_2 for as long as 12 h. Despite this, no hydrogen absorption was registered. We attribute this to a much slower hydriding process consequence of the microstructural changes that occur during the initial desorption at high-temperature [10,30], as well as to a possible surface poisoning [34–36], regardless of manipulating the samples within a glove box at all times. Therefore, both the microstructural changes and the generation of fresh surface consequence of mechanical milling seem to play a crucial role to allow the observation of hydrogen diffusion in MgH_2 at room temperature.

4. Conclusions

MgH_2 formation from Mg and H_2 during mechanical milling, with and without C as an additive, was characterized by *in-situ* pressure measurements. Hydriding has been observed during milling and throughout the rest periods between milling stages. From the analysis of hydrogen absorption during milling, it is concluded that hydriding is controlled by the mechanical process. Additionally it was established that C acts as a process control agent that effectively reduces the mechanical processing time to a half. From the analysis of

hydrogen absorption during the rest periods, it is deduced that the process is controlled by H diffusion in MgH_2. Throughout this process Mg crystallites acts as the effective particles were H diffusion takes place and grain boundaries behave as high-diffusivity paths. From the measured data a lower bound for the diffusion coefficient of H in MgH_2 at room temperature of 10^{-25} m^2 s^{-1} has been estimated.

Acknowledgments

The authors gratefully acknowledge fruitful discussions with J.P. Abriata. They also acknowledge financial support by ANPCyT, and UNCuyo, Argentina.

REFERENCES

[1] Schlapbach L, Züttel A. Hydrogen-storage materials for mobile applications. Nature 2001;414:353–8.
[2] Züttel A. Materials for hydrogen storage. Mater Today 2003;6:24–33.
[3] Sakintuna B, Lamari-Darkrim F, Hirscher M. Metal hydride materials for solid hydrogen storage: a review. Int J Hydrogen Energy 2007;32:1121–40.
[4] Dornheim M, Doppiu S, Barkhordarian G, Boesenberg U, Klassen T, Gutfleisch O. Hydrogen storage in magnesium-based hydrides and hydride composites. Scr Mater 2007;56:841–6.
[5] Varin RA, Czujko T, Wronski ZS. Nanomaterials for solid state hydrogen storage. 1st ed. New York: Springer; 2009.
[6] Jain IP, Lal Chhagan, Jain Ankur. Hydrogen storage in Mg: a most promising material. Int J Hydrogen Energy 2010;35:5133–44.
[7] Aguey-Zinsou K-F, Ares-Fernandez JR. Hydrogen in magnesium: new perspectives toward functional stores. Energy Environ Sci 2010;3:526–43.
[8] Zaluska A, Zaluski L, Ström-Olsen J. Nanocrystalline magnesium for hydrogen storage. J Alloys Compd 1999;288:217–25.
[9] Huot J, Liang G, Boily S, van Neste A, Schulz R. Structural study and hydrogen sorption kinetics of ball-milled magnesium hydride. J Alloys Compd 1999;293-295:495–500.
[10] Fuster V, Urretavizcaya G, Castro FJ. Characterization of graphite catalytic effect in reactively ball-milled MgH_2-C and Mg-C composites. Int J Hydrogen Energy 2011;36:951–61.
[11] Suryanarayana C. Mechanical alloying and milling. 1st ed. New York: Marcel Dekker Inc; 2004.
[12] Chen Y, Williams JS. Formation of metal hydrides by mechanical alloying. J Alloys Compd 1995;217:181–4.
[13] Doppiu S, Schultz L, Gutfleisch O. In situ pressure and temperature monitoring during the conversion of Mg into MgH_2 by high-pressure reactive ball milling. J Alloys Compd 2007;427:204–8.
[14] Dunlap RA, Cheng ZH, MacKay GR, O'Brien JW, Small DA. Preparation of nanocrystalline metal hydrides by ball milling. Hyperfine Interact 2000;130:109–26.
[15] Friedrichs O, Borgschulte A, Züttel A. Controlled mechanically activated hydrogen sorption. Int J Hydrogen Energy 2008;33:5606–10.
[16] Zhang J, Cuevas F, Zaïdi W, Bonnet J-P, Aymard L, Bobet J-L, et al. Highlighting of a Single reaction path during reactive ball milling of Mg and TM by quantitative H_2 gas sorption analysis to form ternary complex hydrides (TM = Fe, Co, Ni). J Phys Chem C 2011;115:4971–9.
[17] Töpler J, Buchner H, Säufferer H, Knorr K, Prandl W. Measurements of the diffusion of hydrogen atoms in magnesium and Mg_2Ni by neutron scattering. J Less-Common Met 1982;88:397–404.
[18] Stioui M, Grayevsky A, Moran A, Kreitzman S, Kaplan N, Shaltiel D. Proton magnetic resonance study of diffusion-related properties in magnesium-rich compounds. J Less-Common Met 1984;104:119–24.
[19] Conradi MS, Mendenhall MP, Ivancic TM, Carl EA, Browning CD, Notten PHL, et al. NMR to determine rates of motion and structures in metal-hydrides. J Alloys Compd 2007;446-447:499–503.
[20] Corey RL, Ivancic TM, Shane DT, Carl EA, Bowman Jr RC, Bellosta von Colbe JM, et al. Hydrogen motion in magnesium hydride by NMR. J Phys Chem C 2008;112:19784–90.
[21] Cermák J, Král L. Hydrogen diffusion in Mg–H and Mg–Ni–H alloys. Acta Materialia 2008;56:2677–86.
[22] Yao X, Zhu ZH, Cheng HM, Lu GQ. Hydrogen diffusion and effect of grain size on hydrogenation kinetics in magnesium hydrides. J Mater Res 2008;23:336–40.
[23] Yang B, He Y-P, Zhao Y-P. Hydrogenation of magnesium nanoblades: the effect of concentration dependent hydrogen diffusion. Appl Phys Lett 2011;98:081905.
[24] Takacs L, McHenry JS. Temperature of the milling balls in shaker and planetary mills. J Mater Sci 2006;41:5246–9.
[25] Hu YQ, Zhang HF, Yan C, Ye L, Ding BZ, Hu ZQ. Hydrogenation mechanisms of Mg during reaction ball milling. J Mater Sci 2004;39:1455–7.
[26] House JE. Principles of chemical kinetics. 2nd ed. Amsterdam: Academic Press; 2007.
[27] Zeng K, Klassen T, Oelerich W, Bormann R. Critical assessment and thermodynamic modeling of the Mg-H system. Int J Hydrogen Energy 1999;24:989–1004.
[28] Manchester FD. Phase diagrams of binary hydrogen alloys. 1st ed. Materials Park: ASM International; 2000.
[29] Fuster V, Urretavizcaya G, Castro FJ. Characterization of MgH_2 formation by low-energy ball-milling of Mg and Mg+ C (graphite) mixtures under H_2 atmosphere. J Alloys Compd 2009;481:673–80.
[30] Paik B, Walton A, Mann V, Book D, Jones IP, Harris IR. Microstructure of ball milled MgH_2 powders upon hydrogen cycling: an electron microscopy study. Int J Hydrogen Energy 2010;35:9012–20.
[31] Polanski M, Bystrzycki J, Plocinski T. The effect of milling conditions on microstructure and hydrogen absorption/desorption properties of magnesium hydride (MgH_2) without and with Cr_2O_3 nanoparticles. Int J Hydrogen Energy 2008;33:1859–67.
[32] Hao S, Sholl DS. Hydrogen diffusion in MgH_2 and $NaMgH_3$ via concerted motions of charged defects. Appl Phys Lett 2008;93:251901.
[33] Hao S, Sholl DS. Selection of dopants to enhance hydrogen diffusion rates in MgH_2 and $NaMgH_3$. Appl Phys Lett 2009;94:171909.
[34] Pedersen AS, Vigeholm B, Kjøller J, Larsen B. The effect of cycling in impure hydrogen on the hydrogen capacity of magnesium powder. Int J Hydrogen Energy 1987;12:765–71.
[35] Bouaricha S, Huot J, Guay D, Schulz R. Reactivity during cycling of nanocrystalline Mg-based hydrogen storage compounds. Int J Hydrogen Energy 2002;27:909–13.
[36] Vons VA, Anastasopol A, Legerstee WJ, Mulder FM, Eijt SWH, Schmidt-Ott A. Low-temperature hydrogen desorption and the structural properties of spark discharge generated Mg nanoparticles. Acta Materialia 2011;59:3070–80.